Hindawi
Advances in Civil Engineering
Volume 2022, Article ID 6718796, 22 pages
https://doi.org/10.1155/2022/6718796

Research Article

Evaluation of the Seismic Behavior Based on the Performance of Special Steel Moment Frames by Modified Energy Method and Force Design Method

Ramin Bagherzadeh, Abolfazl Riahi Nouri, Mohammad Sajjad Massoudi, Mohammad Ghazi, and Farzan Haddad Shargh

Department of Civil Engineering, West Tehran Branch, Islamic Azad University, Tehran, Iran

Correspondence should be addressed to Abolfazl Riahi Nouri; riahinouri.abolfazl@wtiau.ac.ir

Received 14 May 2022; Revised 2 June 2022; Accepted 8 June 2022; Published 8 July 2022

Academic Editor: S. Mahdi S. Kolbadi

Copyright © 2022 Ramin Bagherzadeh et al. This is an open access article distributed under the Creative Commons Attribution License, which permits unrestricted use, distribution, and reproduction in any medium, provided the original work is properly cited.

Although conventional methods in seismic design consider such parameters as force, displacement, and ductility, the behavior of a significant number of structures that have been designed and experienced earthquakes shows that the existing criteria are insufficient and more comprehensive ones should be used. In this regard, the energy-based design method may be considered one of the suitable solutions. This method is based on creating a balance between the input and output energy of structures. It is possible to have a more appropriate estimate of the energy input as well as dissipated energy by the structure and use it in the design of the structure. In the modified energy method that has been used in this study, control of items such as the creation of a soft story, establishment of the Strong-Column Weak-Beam concept, the uniform distribution of loads in the members, the nonconcentration of force and local damage, and simultaneous drift control of the structure with the optimal distribution of plastic hinges have been considered. Also, modifications have been made to the energy balance equation. In this paper, 8-, 16-, and 24-story frames with lateral force resisting system of special steel moment frame have been modified by energy method and compared by the design force method of AISC code. Performance level criteria of the ASCE41-17 code have been applied in the design, and the $P-\Delta$ effects have also been considered in the nonlinear analysis. The results show that, for the frame which is designed by the energy method, the plastic hinges are created in the upper stories and beams; however, in the frame designed by the LRFD method, several plastic hinges are formed in the columns of the upper stories, and a local mechanism is created. Also, in 8- and 16-story structures, the weight of the structure which is designed by the energy method is less than that obtained by the LRFD method. The results also showed that, in contrast to the energy method, the relationships presented in the codes regarding the Strong-Column Weak-Beam rule cannot prevent local and undesirable mechanisms in severe earthquakes.

1. Introduction

Current seismic codes for building design often utilize a force or a displacement-based approach in their implementation. In a force-based approach, a structure is designed to ensure that it possesses sufficient strength to resist the maximum forces imparted to it by gravity and earthquake. In a displacement-based approach, the structure is proportioned to achieve a specified performance level based on the target displacement, defined by strain or drift limits, under a specified level of seismic intensity. A third approach, which is gaining popularity in the earthquake engineering community, is the energy-based approach. In this approach, a design is considered satisfactory if the capacity of a structure to absorb or dissipate energy exceeds its energy demand from an earthquake. Seismic resistance of structures in conventional seismic design methods is considered appropriate when the deformation capacity or resistance limit of the structure is more than the demand of the design earthquake. This is despite the fact that a large portion of the damage which is caused by earthquakes is the result of inelastic cycles. Noting that the energy entering the structure is directly

dependent on its cyclic behavior, the energy concept can be considered an effective tool in seismic-resistant design.

In 1956, Housner, for the first time, applied the concept of energy to study the seismic behavior of structures. Despite the simple relations proposed by Housner, his approach opened the way for the future development of the energy method in the seismic design of the structures. He showed that the spectral velocity curve of structures is stable for most earthquakes over a wide range of periods [1]. In 1988, Akiyama also explored seismic design according to the concept of energy. Akiyama proposed a relation for calculating the input energy per unit mass as a function of the period of the structure [2]. In 1998, Fakhri Niasar and Ghafory Ashtiany stated that the energy parameter is comprehensive and includes all characteristic parameters related to an earthquake. They proposed that, due to the scalar nature of the energy, it is required to collect the amounts of energy related to the various components of the earthquake record, rather than considering the energy of one component of the earthquake record alone [3]. In another investigation conducted in 2000 by Ghafory Ashtiany and Maleki, the seismic energy was studied in several reinforced concrete moment frame structures, and some relationships were proposed for the maximum input energy per unit mass of the structure [4].

In 2003, Ruzi explored the energy concept in seismic design and stated that the dependence of the effect of seismic loading and structural strength on conventional seismic design methods could be a shortcoming [5]. In studies conducted by Mollaioli and Decanini in 2001 and Ye in 2009, the effects of the hysteretic model and the slope of the postyield area in the structure's behavioral model on the input energy spectrum were studied. They concluded that the input energy spectrum was not significant; in this case, if the slope of the postyield area became more, it would reduce the drift and the more uniform distribution of inelastic deformations, leading to more uniform damage [6, 7]. In 2007, Ghodrati Amiri et al. studied the impacts of damping and a strong shock of the earthquake on elastic input energy. They concluded that the input energy to the structure increases by an increase in the strong shock of the earthquake [8]. In 2011, Haddad Shargh and Hosseini studied the optimal stiffness distribution at the height of the building to minimize the seismic input energy. They showed that, for medium-sized structures (up to about 22 stories), the optimal stiffness distribution could be considered parabolic; however, for taller structures, the optimal stiffness distribution at height is similar to a bell-shaped curve. [9].

In 2015, Havaei and Mobedi studied the effects of cradle motion due to the yielded column on the response of steel structures [10]. In 2016, Bemanian and Shakib evaluated the nonlinear behavior of a dual steel moment frame-shear wall system under a set of earthquakes and concluded that the dual steel moment frame-shear wall system could be a suitable system for absorbing a high level of input energy [11]. In 2018, Vahdani et al. studied the impacts of damping as well as ductility on the input energy spectrum. They concluded that changing the ductility coefficient was more influential than changing the damping ratio on the relative input energy spectrum [12]. In 2020, Ucar calculated the input energy in MDOF systems using the input energy responses of ESDOF systems according to each mode of the system. He studied 3-, 5-, and 8-story reinforced concrete frames to NTHAs under eleven earthquakes and found that direct input powers of the ESDOF systems could be effectively used to calculate the input energy in the MDOF system [13]. Tran and Adhikari, in 2021, also used the energy-based seismic design process (EBSD) to estimate the SDF and then compared it to the resistance-based SDF. They used the energy method to quantify the performance of the building system [14]. Meanwhile, Baqherzadeh et al., in 2022, using the combination of the energy method and whale metaheuristic optimization (E-WOA) algorithm to optimize steel moment frames, showed that using the E-WOA method improves the plastic hinge distribution and seismic energy dissipation. The structure's weight was also reduced [15].

The main goal of the present study is to apply the energy method to balance the input-output energy of the structure in the special steel moment frame design. In the proposed energy method, the design of the members is carried out by equalizing the structure's input energy and the energy which is dissipated in the plastic hinges. The system's dissipated energy is the result of the energy dissipated at all hinges formed on the frame. In the equilibrium relations, the effects of gravity loads and the higher modes on the energy entering the structure are seen. Based on this balance of energy, the minimum required bending moments of the beams are obtained; based on that, the beams will be designed. The columns will be also designed according to the maximum required capacity and the control of constraints such as Strong-Column Weak-Beam and soft and weak story. By considering all results together, a proper comparison has been made between the responses in the linear and nonlinear regions of the diagram. These relationships have been investigated in special steel moment frames with a different number of stories. The study models are special moment frames of 8, 16, and 24 stories. The story drift and the beam deformations are controlled based on AISC2016 [16]. Furthermore, a pushover analysis is carried out with constant gravity loads and incremental lateral loads. Then, the structure is analyzed nonlinearly with a uniform distribution, and the structures are controlled at four functional levels in the target displacement. The control criteria for this stage are taken from the ASCE41-17 code [17]. The required codes are written in MATLAB [18], and the static linear and nonlinear modeling analyses are carried out in SAP2000 [19]; these two programs are linked.

2. Modified Energy-Based Design Method in Steel Frames

The concept of the energy-based design method is founded on the assumption that the amount of energy required to push a given structure to reach the target displacement equals the maximum input energy of the earthquake, which is approximated by $1/2\gamma M \times S_v^2$ [20, 21].

In the new energy method presented in this paper, the following modifications have been applied to improve the results:

(1) The damping effect of hysteresis cycles has been considered in equilibrium.
(2) The effects of different modes have been seen in the input energy of the earthquake.
(3) A correction factor called γ, which is the ratio of the energy absorbed by the inelastic system to that of the equivalent elastic system, has been considered in the algorithm.
(4) Target displacement is considered as displacement in equilibrium.
(5) The $P-\Delta$ effect has been considered in calculating the base shear.

The energy balance equation proposed by Lee and Goel is as follows [20, 21]:

$$E_e + E_P = \frac{1}{2}\gamma M S_v^2, \tag{1}$$

where E_e and E_P are, respectively, the elastic and plastic components of the energy needed as the structure is pushed up to the target drift. γ is the correction factor, M is the total structure's seismic weight, and S_v is the design pseudovelocity. The researchers have stated thatγ is associated with the natural period of the structure. Also, the period of the structure can have an important impact on the input energy of the ground motion [22].

Figure 1 represents the relationship between the base shear (CW) and the corresponding drift (Δ) for an elastic, as well as an elastoplastic system. Equation (1) can be written as

$$\gamma \frac{1}{2} C_{eu} W \Delta_e = \left(\frac{1}{2} C_y W \left(2\Delta_{\max} - \Delta_y\right)\right). \tag{2}$$

Equation (2) can be summarized as follows:

$$\frac{\gamma \Delta_e}{\Delta_y} = \frac{\left(2\Delta_{\max} - \Delta_y\right)}{\Delta_e}, \tag{3}$$

where $\Delta_e = R_\mu \Delta_y$ and $\Delta_{\max} = \mu_s \Delta_y$. By considering these values in equation (3), one gets the following:

$$\gamma = \left(\frac{2\mu_s - 1}{R_\mu^2}\right). \tag{4}$$

In relation to (4), μ_s is the structure's ductility coefficient, R_μ is the reduction coefficient of ductility, which is related to μ_s, and Δ_y is the yield displacement of the system. In this study, the relationships which have been presented by Newmark and Hall [23], as shown in Table 1, are used.

For multi-degree-of-freedom systems, all vibration frequencies are effective in calculating the seismic input energy [24]. The input energy of multi-degree-of-freedom systems can be written according to (5) [24]:

$$E = \sum_{n=1}^{N} \Gamma_n^2 . E_{SDOF,n}. \tag{5}$$

Γ_n, the modal participation factor for the mode n, is calculated from equation (6):

$$\Gamma_n = \frac{L_n}{M_n^*} \quad L_n = \phi_n^T M l \quad M_n^* = \phi_n^T M \phi_n, \tag{6}$$

where ϕ_n is the vector of the eigenvalues and M refers to the mass matrix. According to the following equation, the input energy of a system is calculated as one degree of freedom, $E_{SDOF,n}$ [24].

$$E_{SDOF,n} = \frac{1}{2}\gamma M_n^* V_{\mathrm{MAX},n}^2 = \frac{1}{2}\gamma M_n^* S_{v,n}^2 = \frac{T_n^2}{8\pi^2}\gamma M_n^* S_{a,n}^2, \tag{7}$$

where $S_{v,n}$ and $S_{a,n}$ refer to the spectral velocity and the spectral acceleration of each mode obtained from the elastic response spectrum. T_n is the nth mode period. In dissipation systems with a decreasing behavior in deformation cycles, there are major cycles that control the input energy of these systems.

Akiyama [2] revealed that the elastic energy for a single degree of freedom (SDOF) could be written as equation (8) with acceptable accuracy:

$$E_e = \frac{1}{2} V_y \Delta_y = \frac{1}{2} M \left(\frac{T_e}{2\pi} \cdot \frac{V_y}{W} g\right), \tag{8}$$

where V_y refers to the yield base shear, Δ_y indicates the yield displacement limit, T_e is the structure's period, g denotes the gravitational acceleration, and W is the weight of the structure.

The frame's yield mechanism is assumed as represented in Figure 2. Frame's plastic deformation occurs after the structure reaches the yield point.

According to Hazner's assumption, the energy which enters the structure is equal to the sum of elastic and plastic energy [25]. According to equation (9), Leelataviwat et al. [26] proposed an energy-based approach to the performance-based design in which the need for drift control was eliminated at the end of the design. The concept of energy balance is shown in Figure 3.

$$E_e + \eta E_p = \lambda E, \tag{9}$$

where E refers to the input energy to the structure, E_e is the elastic energy, and E_p is the energy dissipated by plastic hinges. λ and η are the damping coefficients and the behavior of the curve representing the deformation cycle of the structure, respectively.

The value λ was considered equal to$\lambda = 1/1 + 3\xi + 1.2\sqrt{\xi}^2$ by Akiyama [2]; ξ is the damping of the structure.

In this paper, equation (9) has been used to modify plastic energy, and equation (1) has been applied to modify the earthquake's input energy. Finally, the modified energy balance equation is as follows:

$$E_e + \eta E_p = \gamma E. \tag{10}$$

To define η according to Figures 4(a) and 4(b), the effects of earthquake reciprocating behavior on sections can be seen through equation (11) [27]:

$$\eta = \frac{A_P}{A_F} = \frac{A_P}{A_F} \cdot \left(\frac{A_F}{A_{RPP}}\right)^{-1}. \tag{11}$$

This relationship is defined for the quantification of the energy dissipation capacity of structural systems with

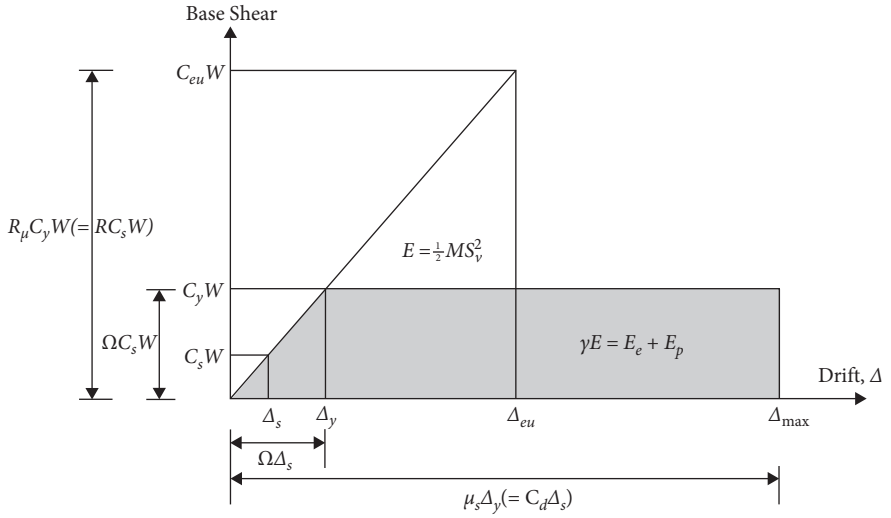

Figure 1: Structural idealized response and energy balance concept [22].

Table 1: Ductility reduction factor and the corresponding structural period range.

Period range	Ductility reduction factor
$0 \le T \le T_1/10$	$R_\mu = 1$
$T_1/4 \le T \le T_1/10$	$R_\mu = \sqrt{2\mu_s - 1}\,(T_1/4T)^{2.315\log(1/\sqrt{2\mu_s-1})}$
$T_1/4 \le T \le T_1'$	$R_\mu = \sqrt{2\mu_s - 1}$
$T_1' \le T \le T_1$	$R_\mu = T\mu_s/T_1$
$T_1 \le T$	$R_\mu = \mu_s$
$T_1 = 0.57\,\text{sec}\ T_1' = T_1(\sqrt{2\mu_s - 1}/\mu_s)\text{sec}$	

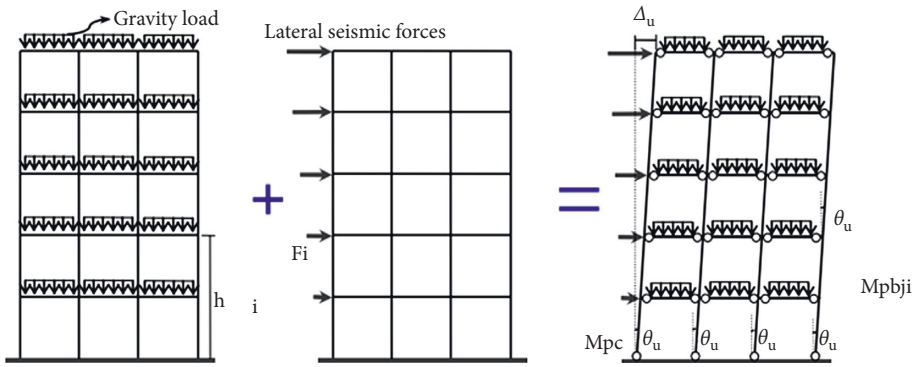

Figure 2: A frame's yield mechanism [24].

reduced hysteresis cycles. As can be seen, the A_F and A_{RPP} values are constant, and η coefficient is a function of A_P.

According to Figure 4(b), the real hysteresis rings of structures are not complete; this means that they are reduced or compressed in some areas. For such structures, to calculate inelastic strain energy, according to Figure 4(a), the energy dissipation capacity is overestimated. Therefore, to improve the energy-based plastic method for designing structural frames, the effect of reducing the area enclosed to the structural hysteresis cycle must be considered. In Figure 4, A_P is the area enclosed by the reduced hysteresis cycle. A_{RPP}/A_F can be written as follows [27]:

$$\frac{A_F}{A_{RPP}} = \frac{(\mu - 1)(1 - r)}{\mu(1 + r\mu - r)}. \tag{12}$$

In this relation, r is the slope of the second part of the ratio of hardness, and μ is the ductility factor ($\mu = \Delta_{\max}/\Delta_y$), where $\Delta_{\max}$ refer to the maximum displacement and Δ_y indicates the yield point. The consumed energy in each plastic hinge is determined based on the type of its cyclic behavior. In this research, the Takada model has been applied as follows [27]:

$$\xi_H = \frac{2}{\pi}.\frac{A_P}{A_{RPP}} \Rightarrow \frac{A_P}{A_{RPP}} = \frac{\pi}{2}.\xi_H \Rightarrow \eta = \frac{\pi\mu(1 + r\mu - r)}{\mu(\mu - 1)(1 - r)}, \tag{13}$$

where ξ_H is hysteretic damping. For the type of cycle and the effect of periodicity, Dwairi et al. [27] presented the damping equation according to (14):

$$\xi_H = C\left(\frac{\mu - 1}{\pi\mu}\right) \Rightarrow \eta = C.\frac{(1 + r\mu - r)}{2(1 - r)}. \tag{14}$$

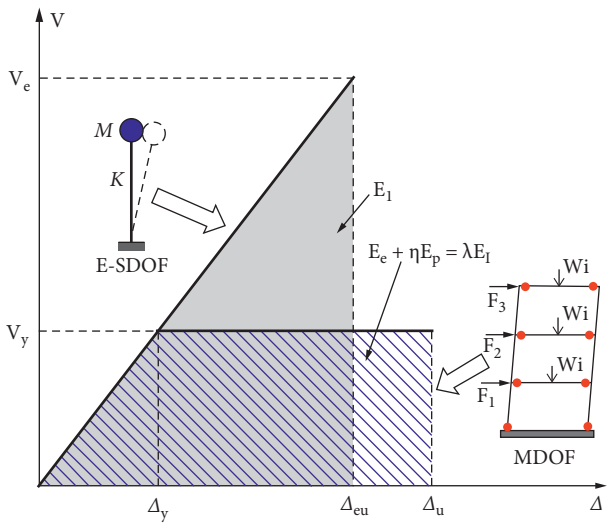

Figure 3: The concept of energy balance [26].

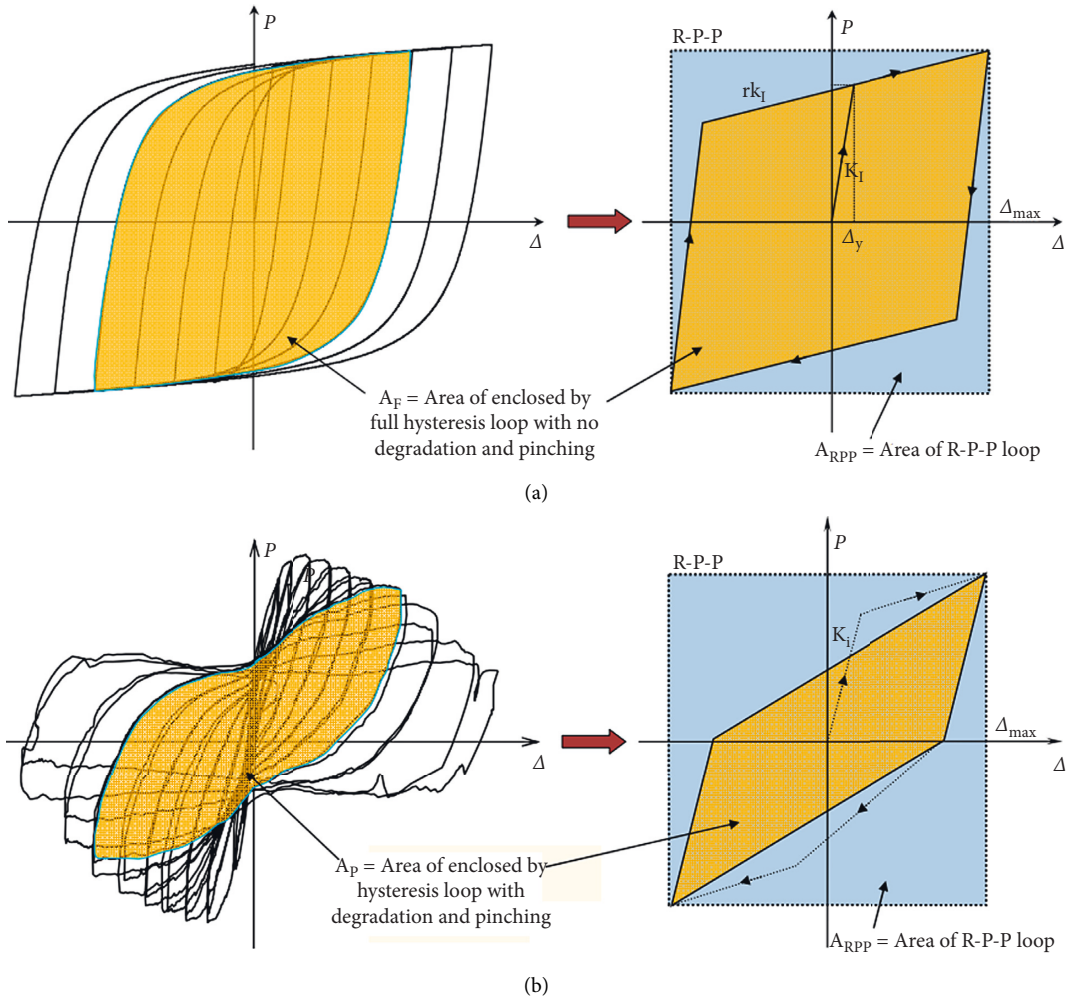

Figure 4: Effects of earthquake reciprocating behavior on sections [27]. (a) The hysteresis cycle and its equivalent model. (b) Reduced hysteresis and its equivalent model.

In this relation, the value of C was suggested based on equation (15) and the elastoplastic model:

$$C = \begin{cases} 0.85 + 0.6\left(1 - T_{eff}\right), & for \quad T_{eff} < 1s, \\ 0.3, & for \quad T_{eff} \geq 1s, \end{cases} \tag{15}$$

where T_{eff} is the main rotation of the structure.

According to equations (1), (7), (8), and (10), the total plastic energy a structure must dissipate during an earthquake for a given system with multidegrees of freedom is equal to

$$E_P = \frac{\gamma E - E_e}{\eta} = \left(\lambda . \sum_{n=1}^{N} \Gamma_n^2 . \left(\frac{T_n^2}{8\pi} M_n^* S_{a,n}^2 \right) - \frac{1}{2} M . \left(\frac{T_e}{2\pi} . \frac{V_y}{W} g \right)^2 \right) . \eta^{-1}. \tag{16}$$

The rotation related to the plastic area of the frame (θ_p) will be equal to the difference existing between the total elastic and plastic rotation of the frame and the elastic rotation. In this paper, nonlinear static analysis is performed to accurately determine θ_p. Also, the rotation of a point on the curve whose slope changes is considered as the value of the elastic rotation.

The energy obtained from equation (16) must be dissipated by the plastic hinges shown in Figure 3, which is equal to

$$E_P = \left((m+1) M_{pc} + 2 \sum_{j=1}^{m} \mu_j \sum_{i=1}^{n} \beta_i M_{pbr} \right) \theta_p, \tag{17}$$

where M_{pbr} refers to the reference moment of the plastic beam at the jth opening, M_{pc} indicates the plastic moment of the base of the columns on the first story, m represents the number of frame openings, n stands for the number of frame stories, and β_i is the coefficient of the resistance distribution of the beams (the value of which is mentioned below) on the 1st story. Also, $\mu_j = l_r / l_j$ is the reference moment coefficient of the beams, which equals the ratio of the length of the reference opening to the length of the jth opening.

After yield, the external forces should be in equilibrium with the internal ones. By equating the energy dissipated in the plastic state with the external one, which is done by lateral forces and gravitational loads, we can act according to equation (18):

$$E_P = V_y \left(\frac{\sum_{i=1}^{n} W_i h_i^{k+1}}{\sum_{i=1}^{n} W_i h_i^k} \right) \theta_p + \sum_{i=1}^{n} W_i \frac{\theta_p^2 h_i}{2}. \tag{18}$$

To obtain the frame's base shear with a suitable estimation, the input energy of the dissipated earthquake (by equation (16)) can be equal to the work which is done by external forces (on plastic hinge), which includes lateral and gravitational loads according to equation (19).

$$V_y \left(\frac{\sum_{i=1}^{n} W_i h_i^{k+1}}{\sum_{i=1}^{n} W_i h_i^k} \right) \theta_p + \sum_{i=1}^{n} W_i \frac{\theta_p^2 h_i}{2} = \left(\gamma . \sum_{n=1}^{N} \Gamma_n^2 . \left(\frac{T_n^2}{8\pi} M_n^* S_{a,n}^2 \right) - \frac{1}{2} M . \left(\frac{T_e}{2\pi} . \frac{V_y}{W} g \right)^2 \right) . (\eta)^{-1}, \tag{19}$$

where K is equal to

$$\begin{aligned} K &= 0.5T + 0.75, \\ if\ T \leq 0.5 &\longrightarrow k = 1, \\ if\ T \geq 2.5 &\longrightarrow k = 2. \end{aligned} \tag{20}$$

In the base shear relation, as calculated by the energy method, the effects of $P - \Delta$ are not considered. To apply the effects of $-\Delta$, we can use its value by adding its value to the lateral loads of equation (21).

$$F_i^p = F_i + \Delta F_i = \alpha_i V_y + W_i \theta_u, \tag{21}$$

where ΔF_i is the additional lateral load due to gravity loads, F_i refers to the seismic force at the level i, W_i is the weight of the story level, θ_u is the angle of the rotation of the story, and α_i is the ratio of the lateral force, which is distributed at the story level to the base shear.

By solving the quadratic equation of equation (19), the base shear value will be obtained. Once the base shear is determined, the design force of each level is obtained.

To calculate the beam's M_{pbr}, the columns plastic moment, M_{pc}, must be properly estimated. This appropriate value is determined by imposing the prevention of the formation of soft-story failure in the first story. For this purpose, plastic hinges at the top and bottom of the first-story columns are assumed. The story columns' plastic moment capacity is determined to prevent the formation of this failure state according to Figure 5.

$$M_{pc} = 1.1 \left(\frac{V_y h_1 + W h_1 \theta_p}{2(m+1)} \right). \tag{22}$$

The parameters of this relation have been introduced before, and the factor 1.1 is the overstrength factor to account for possible overloading due to strain hardening [28].

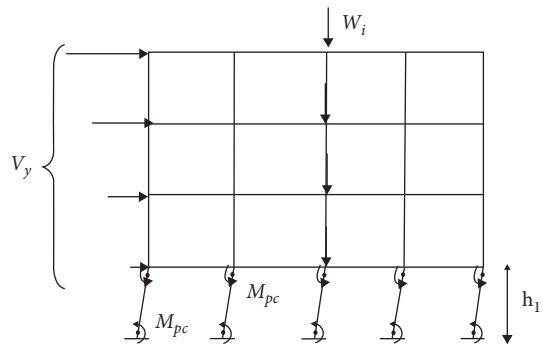

Figure 5: Soft-story failure mode.

The coefficient of resistance distribution, β_i, plays a significant role in structures' seismic response. This coefficient depends on the structures' hardness as well as lateral strength along the height. β_i must be properly selected to match the forces exerted during the earthquake. It also ensures that the incoming energy is dissipated in the structure, thus preventing damage from being concentrated on one story. Numerous numerical analyses have been previously conducted to obtain the best resistance distribution of the beams. The aim was to obtain a function that could well express the shear resulting from different earthquakes. As an initial approximation, the relative distribution of shear force at height during an earthquake can be approximated by the distribution of static shear force at height, as calculated from (23). Its value is equal to [29]

$$\beta_j = \left(\frac{V_i}{V_y}\right)^{1/2}, \tag{23}$$

where V_i and V_y are static shear in the ith level and the highest story level, respectively. The value of 1/2 is obtained using the least-squares method from the results which are obtained from several nonlinear dynamic analyses [29]. By establishing the equation of relations (17) and (18) and getting its unknowns, the value of M_{pbr} is obtained; then, based on that value, the design moment of the beams is calculated, as represented as follows:

$$\varphi M_{pbij} \geq \mu_j \beta_i M_{pbr}, \tag{24}$$

where φ refers to the resistance coefficient, and it is calculated based on AISC2016 [17]. M_{pbij} indicates the beam's plastic moment in the ith story and the jth opening.

3. Nonlinear Static Analysis

The finite element planar model related to the three steel frames described above was established by applying the SAP2000 software [20]. The finite element model is shown in Figures 6 and 7 (taking the 8-story steel frame as an example). The frame sections are adopted for all beams and columns. Each of the beams and columns includes only one element with two nodes. All steel frames are well connected. The column base is fixed too.

The finite element planar model was established completely, and then the related pushover analyses were carried out. The hinge P-M3 was then applied for the simulation of the frame columns' material nonlinearity. Also, the use was made of the hinge M3 to simulate the frame beams nonlinearity. The constitutive relation related to the hinge P-M-M can be seen in Figure 7. The vertical coordinate shows the bending moments, while the horizontal one represents the rotation. Plastic hinges' mechanical behavior can be determined according to ASCE41-17 [18]. In the pushover analysis, the material strength uses the average values, and the lateral force applies the inverted triangular distribution pattern.

For the nonlinear static method, the general relationship of the deformation force, as represented in Figure 8, can be used. The effects of strain hardening are considered by assuming a slope, which is equal to 3% of the slope of the elastic part. Details of this figure are given in ASCE41-17 [18].

The pushover analysis was done in accordance with ASCE41-17 [18]. To apply the combination of gravity loads and lateral load distribution patterns, in the combination of gravity and lateral loads, the upper and lower limits of gravity load effects, Q_G, were calculated from the relations (25) and (26).

$$Q_G = 1.1\left(Q_D + Q_L\right), \tag{25}$$

$$Q_G = 0.9Q_D, \tag{26}$$

where Q_D and Q_L are the effective seismic dead and live loads, respectively.

In the section related to examples and numerical results, to compare the results, all two methods were analyzed and examined based on nonlinear static analysis.

In the optimization process, target displacement for each of the candidate designs is computed by applying equation (27) to conduct the pushover analysis.

$$\delta_t = C_0 C_1 C_2 S_a \frac{T_e^2}{4\pi^2} g, \tag{27}$$

where C_0, C_1, and C_2 factors are determined on the basis of ASCE41-17 [18]. The structural effective fundamental period is shown by T_e, and the ground motion acceleration is indicated by g. Also, S_a denotes the spectral acceleration

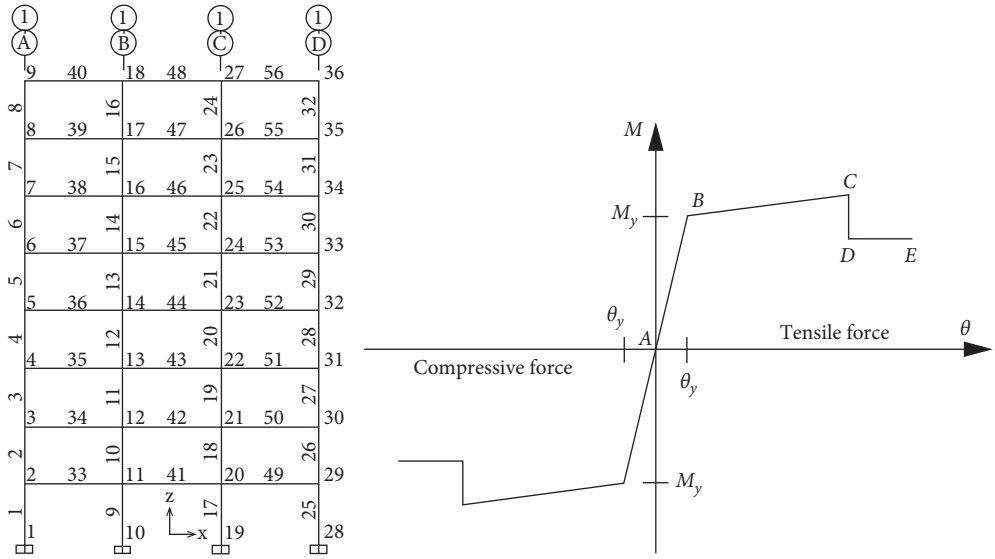

Figure 6: The 8-story steel frame's finite element planar model.

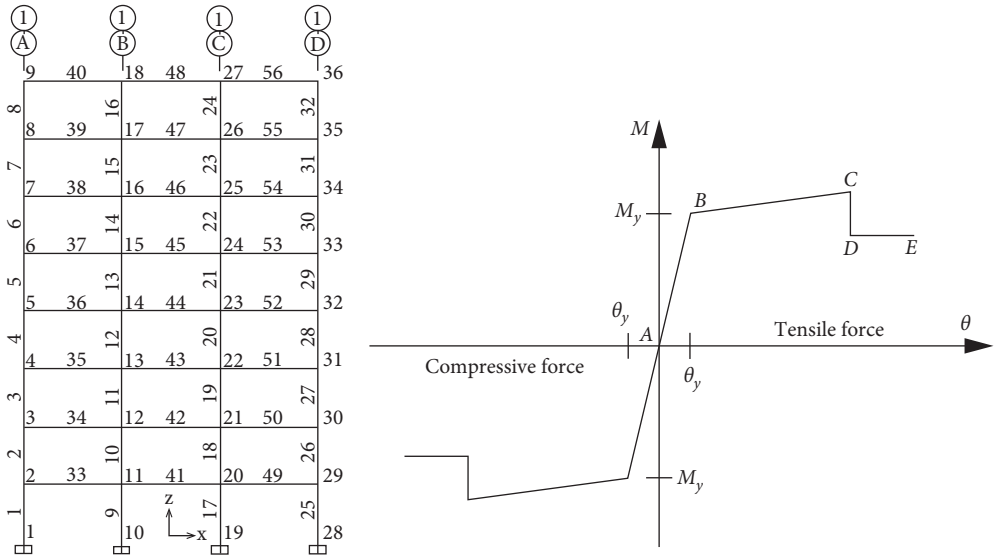

Figure 7: Constitutive relation of the hinge P-M-M.

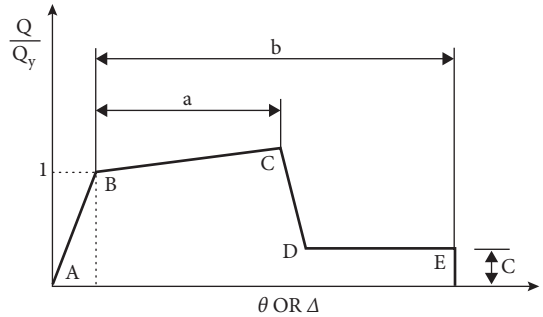

Figure 8: General force-deformation curve for members and components.

which is estimated according to the ASCE41-17 code [18]. The analysis is according to the assumption that the roof target displacement is equal to 0.004, 0.007, 0.025, and 0.05, relative to the structure's total height. Each of these values represents the performance levels of OP, IO, LS, and CP. Control of the story drift is done for all functional levels;

however, the members' permissible rotation is checked for the last three target movements.

After performing a nonlinear analysis and getting the required results, the constraints are checked as follows:

(a) For beams, according to the slenderness ratio, the constraint related to the member's rotation is controlled through equation (28).

$$\theta_{beam} \leq \theta^{i}_{all} \quad i = OP, IO, LS, CP. \tag{28}$$

In this relation, θ^{i}_{all} is equivalent to the rotation of the beam at its end, and θ_{beam} is the permissible displacement in ASCE41-17 [18], according to the desired level of performance.

For columns, based on the displacement of the control, the permissible rotation must be controlled by relation (29). According to the control force, the control of the force ratio in the final stage of the analysis related to the column capacity should be done based on equation (30).

$$\theta_{column} \leq \theta^{i}_{all} \quad i = OP, IO, LS, CP, \tag{29}$$

$$\frac{P_c}{\phi P_n} + \frac{M_c}{\phi M_n} \leq 1. \tag{30}$$

In this relation, P_c and ϕP_n refer to the axial force and the nominal capacity of the column, respectively. Further, M_c and ϕM_n indicate the columns' present bending moment and nominal capacity, respectively. θ_{column} is also permissible displacement in ASCE41-17 [17] according to the desired performance level.

Story drift constraint can be controlled according to relation (31):

$$\Delta^{i}_{\text{inter}story} \leq \Delta^{i}_{all\text{interstory}}, \tag{31}$$

where $\Delta^{i}_{\text{interstory}}$ is the story drift based on the desired performance level and $\delta^{i}_{all\text{interstory}}$ refers to the allowable story drift in OP to CP performance levels.

Strong-Column Weak-Beam constraint is defined as shown in relation (32):

$$\frac{\sum M_{P\text{column}}}{\sum M_{P\text{beam}}} \geq 1. \tag{32}$$

Based on this relation, $M_{P\text{column}}$ and $M_{P\text{beam}}$ refer to the plastic moment of the columns and beams, respectively.

The flowchart of the modified energy method is shown in Figure 9.

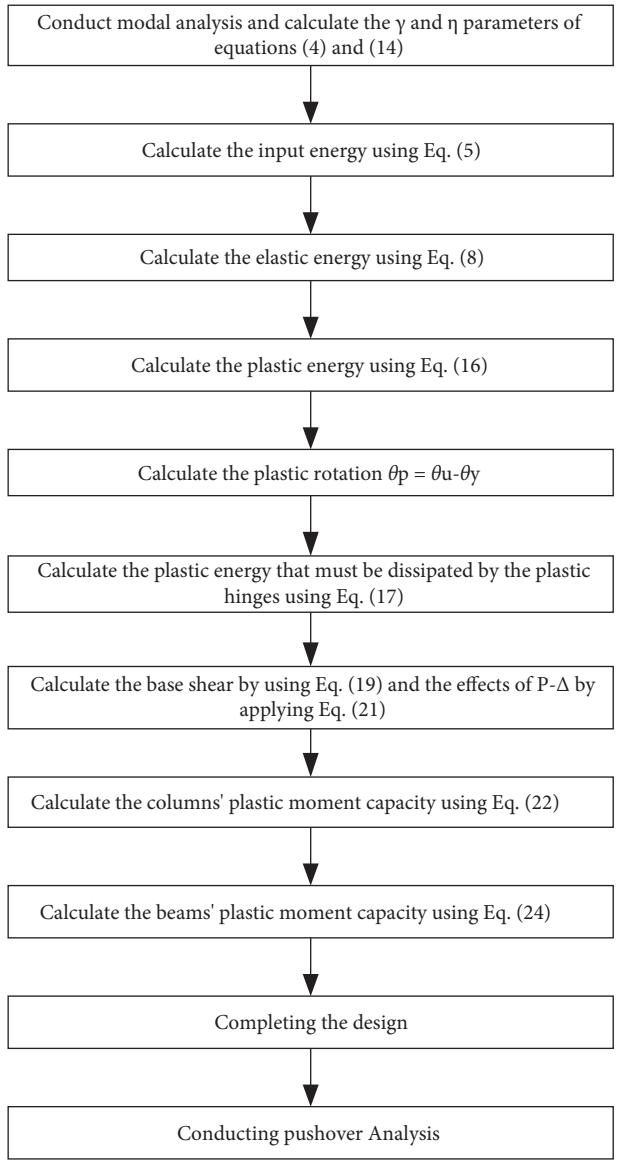

Figure 9: Flowchart of the modified energy method.

4. Numerical Examples

4.1. Introducing Steel Frame Models and Controlling Structural Design Criteria. In the present study, three two-dimensional 8-, 16-, and 24-story frames were modeled to compare different design methods. The number of spans, the length of each span, and the height of the stories were 5, 5, and 3 meters, respectively. The dead and live loads on the stories were 5000 and 2000 kg/m, respectively. All sections used in the modeling were selected from W-shaped sections of the AISC database [17]. The important point that has been observed in the selection of sections was that all selected sections had seismic compression conditions. The specifications of the steel materials modeled in this paper are as described in Table 2.

Seismic loading in the static analysis of structures was done based on ASCE7-16 [29]. For designing by the LRFD method, the design location of the frames in an area with the soil class *D* (an area with a very high relative risk) was assumed, and residential use was considered for the buildings. According to ASCE 7-16 standards [29], the coefficient $S_1 = 0.63$ and the coefficient $S_s = 1.5$ were considered. A permissible relative displacement control of 0.02 was used for the structures. The modeling and design of the frame were carried out using the LRFD method by applying the SAP2000 software [19].

In structural models, the lateral load-resistant system is a special steel moment frame, and all nodal connections of the structures are rigid.

Table 2: Specifications of the steel materials.

$W = 7850 kg/m^3$	Unit weight of the material volume
$E = 2.0e + 10 kgf/m^2$	Modulus of elasticity
$\nu = 0.3$	Poisson's ratio
$F_y = 24e + 6 kgf/m^2$	Stress yield of steel materials
$F_u = 37e + 6 kgf/m^2$	Ultimate tensile stress of steel materials

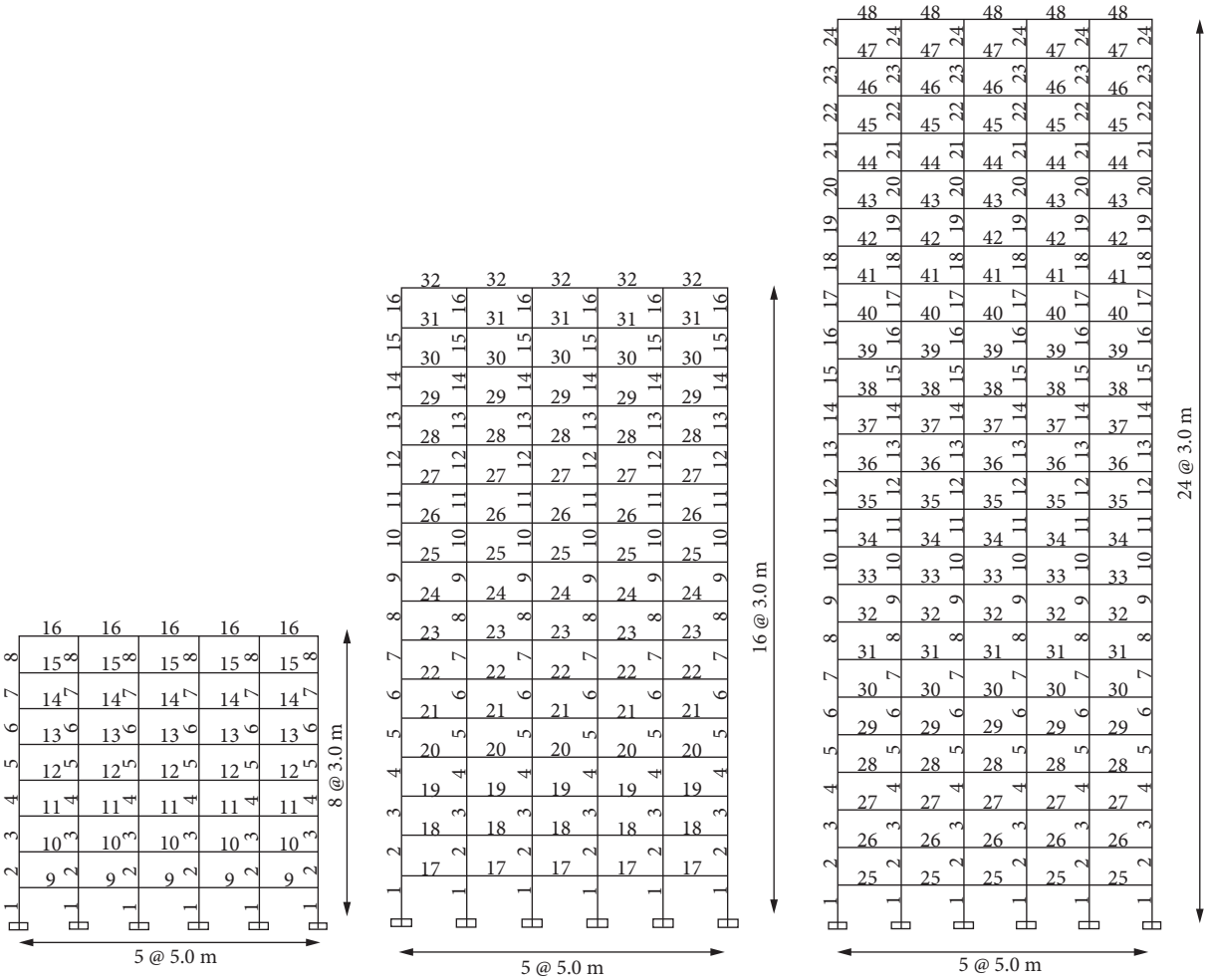

Figure 10: Typology of the designed models of 8-, 16-, and 24-story structures.

The codes related to the energy method have been written in the MATLAB software [18]. The nonlinear static analyses of the frames were performed in the SAP2000 software [18], and SAP2000 software [19] was linked to the MATLAB software [18]. Different types of sections are shown in Figure 10. Also, the section specifications of the two methods are represented in Tables 3 to 5.

The results related to the energy and LRFD methods in shifting the target locations IO, LS, and CP were obtained. The results of shifting the target location LS are presented as the design results obtained through these methods. Also, the final result is presented for all three examples according to Tables 3–5 for the LRFD and energy methods.

4.2. Controlling the Results of Frame Analyses. After designing the structure in accordance with the AISC 2016 standard [16] and performing all controls required by the codes, the ratio of the minimum, maximum, and average stress of members and the ratio of the capacity of beams to columns are shown in Tables 6–8.

One of the most important controls performed on a special moment frame or a highly ductile moment frame is the Strong-Column Weak-Beam control. According to this rule, the plastic hinge should be formed first in the beams; then, the structure can withstand further deformation without any reduction of strength. As can be seen from the above tables, the capacity of the beams to the

Table 3: Final design results of energy and LRFD methods in 8-story structures.

Type number and cross section assigned to each of the beams and columns of the frame													Design methods
13	12	11	10	9	8	7	6	5	4	3	2	1	
W12 × 79	W14 × 74	W14 × 74	W14 × 74	W14 × 74	W16 × 36	W24 × 84	W27 × 102	W27 × 102	W30 × 148	W30 × 148	W30 × 148	W36 × 160	LRFD
W21 × 50	W21 × 55	W21 × 55	W24 × 55	W24 × 55	W21 × 55	W24 × 76	W30 × 90	W27 × 84	W30 × 90	W30 × 108	W33 × 118	W33 × 130	Energy
										16	15	14	
										W10 × 54	W10 × 54	W12 × 79	LRFD
										W14 × 37	W18 × 40	W21 × 44	Energy

Table 4: Final design results of energy and LRFD methods in 16-story structures.

Type number and cross section assigned to each of the beams and columns of the frame													Design methods
13	12	11	10	9	8	7	6	5	4	3	2	1	
W33 × 169	W33 × 169	W33 × 169	W33 × 201	W33 × 201	W33 × 201	W33 × 201	W33 × 201	W33 × 201	W33 × 201	W36 × 210	W36 × 230	W36 × 328	LRFD
W33 × 130	W40 × 149	W40 × 167	W40 × 189	W40 × 199	W40 × 215	W44 × 230	W44 × 230	W44 × 262	W44 × 262	W44 × 262	W44 × 290	W44 × 290	Energy
26	25	24	23	22	21	20	19	18	17	16	15	14	
W14 × 74	W14 × 74	W16 × 67	W16 × 67	W16 × 67	W16 × 67	W16 × 67	W16 × 67	W16 × 67	W16 × 67	W27 × 129	W27 × 129	W33 × 169	LRFD
W21 × 50	W21 × 50	W21 × 55	W21 × 55	W21 × 55	W21 × 55	W21 × 55	W21 × 55	W21 × 55	W21 × 55	W21 × 50	W27 × 84	W30 × 108	Energy
							32	31	30	29	28	27	
							W10 × 54	W12 × 58	W12 × 58	W14 × 74	W14 × 74	W14 × 74	LRFD
							W16 × 31	W18 × 35	W18 × 40	W21 × 44	W21 × 44	W18 × 50	Energy

Table 5: Final design results of energy and LRFD methods in 24-story structures.

Type number and cross section assigned to each of the beams and columns of the frame													Design methods
13	12	11	10	9	8	7	6	5	4	3	2	1	
W40 × 372	W40 × 372	W40 × 372	W40 × 372	W40 × 372	W40 × 397	W40 × 397	W40 × 397	W40 × 397	W40 × 431	W40 × 431	W40 × 431	W40 × 431	LRFD
W40 × 372	W40 × 397	W40 × 431	W40 × 503	W40 × 503	W40 × 503	W40 × 503	W40 × 593	W40 × 593	W40 × 593	W40 × 593	W40 × 593	W36 × 650	Energy
26	25	24	23	22	21	20	19	18	17	16	15	14	
W18 × 86	W18 × 86	W21 × 93	W27 × 114	W27 × 114	W30 × 148	W30 × 148	W33 × 169	W33 × 263	W33 × 263	W33 × 263	W40 × 277	W40 × 277	LRFD
W21 × 68	W21 × 68	W21 × 55	W30 × 90	W33 × 130	W40 × 149	W40 × 183	W40 × 211	W44 × 230	W44 × 262	W44 × 290	W40 × 324	W44 × 335	Energy
39	38	37	36	35	34	33	32	31	30	29	28	27	
W16 × 77	W16 × 77	W18 × 76	W18 × 76	W18 × 76	W18 × 76	W18 × 76	W18 × 76	W18 × 76	W18 × 76	W18 × 76	W18 × 86	W18 × 86	LRFD
W21 × 62	W21 × 62	W24 × 62	W24 × 62	W24 × 62	W24 × 62	W21 × 68	W21 × 68	W21 × 68	W21 × 68	W21 × 68	W21 × 68	W21 × 68	Energy
				48	47	46	45	44	43	42	41	40	
				W12 × 58	W12 × 58	W12 × 58	W12 × 58	W16 × 77	W16 × 77	W16 × 77	W16 × 77	W16 × 77	LRFD
				W16 × 31	W16 × 40	W21 × 44	W18 × 50	W21 × 50	W21 × 55	W21 × 55	W24 × 55	W24 × 55	Energy

Table 6: Results of the analyses of LRDF, energy, and E-WOA methods in 8-story structures.

Average capacity of beams to columns	Minimum capacity of beams to columns	Maximum capacity of beams to columns	Average stress ratio	Minimum stress ratio	Maximum stress ratio		Design methods
0.8669	0.6357	0.9664	0.7243 0.7006	0.5541 0.3723	0.9398 0.9346	Beams Columns	LRFD
0.8492	0.3757	1. 0	0.7655 0.6882	0.5634 0.3155	0.9722 1.011	Beams Columns	Energy

Table 7: Results of the analyses of LRDF, energy, and E-WOA methods in 16-story structures.

Average capacity of beams to columns	Minimum capacity of beams to columns	Maximum capacity of beams to columns	Average stress ratio	Minimum stress ratio	Maximum stress ratio		Design methods
0.5278	0.01	0.9039	0.7703 0.6650	0.5321 0.3234	0.9438 0.9793	Beams Columns	LRFD
0.310	0.01	0.7412	0.8532 0.5619	0.5126 0.2845	1.018 0.8175	Beams Columns	Energy

Table 8: Results of the analyses of LRDF, energy, and E-WOA methods in 24-story structures.

Average capacity of beams to columns	Minimum capacity of beams to columns	Maximum capacity of beams to columns	Average stress ratio	Minimum stress ratio	Maximum stress ratio		Design methods
0.2722	0.01	0.6528	0.8064 0.5301	0.4388 0.2242	0.9621 0.9394	Beams Columns	LRFD
0.1937	0.01	0.6812	0.8429 0.4333	0.4691 0.2395	1.00 0.6505	Beams Columns	Energy

columns in the energy method is, on average, lower than that in the LRFD methods.

4.3. Lateral Displacement Control of the Structure. Lateral displacement control of the structure is performed according to the clause 12.12.1 of the ASCE7-16 code [29]. Accordingly, the relative nonlinear lateral displacement of the story, δ_M, will be calculated by equation (33). In this relation, C_d refers to the magnification coefficient of the structure's lateral displacement owing to the nonlinear behavior, δ_{xe} indicates the relative linear displacement of the story, and I_e is the coefficient of the importance of the building.

$$\delta_M = \frac{C_d \times \delta_{xe}}{I_e}. \tag{33}$$

The value of δ_M, as obtained by considering the effects of $-\Delta$, should not exceed the allowable value of equation (34). In the above relation, h_{sx} is the story height.

$$\Delta_a = 0.02h_{sx}. \tag{34}$$

Figure 11 shows the relative lateral displacement diagrams of 8-, 16-, and 24-story structures using the energy and LRFD methods.

5. Results of the Nonlinear Static Analysis of Frames

In all three examples, following the design of the structures by energy and LRFD methods, for the purpose of comparison, after adjusting the plastic hinges of the frame members and conducting nonlinear static analysis, dead and live loads are applied as the dynamic loads; by continuing to apply gravitational loads, pushing of structures is done with the lateral static load pattern introduced in the paper. The frames are pushed to a greater displacement than the target displacement and to the point to better study the behavior of the structure and the formation of plastic hinges.

5.1. Example 1: 8-Story Frame. Figure 12 shows the plastic hinges created on 8-story frames designed by the energy and LRFD methods.

Figures 13 and 14 have been applied to better understand the process of forming plastic hinges on the frames. In these figures, on the diagram, the pushing images of plastic hinge formation in different stages are shown.

According to the diagram represented in Figure 13, which is related to the LRFD method, the poor performance of the frame in the nonlinear range can be seen. Also, in the initial stages, the pushing of the side column of the second story has entered its nonlinear state; then, the other columns of this story and the last one have also entered the nonlinear state. However, the optimal position for the frame mechanism is the plastic hinge of the two ends of all beams; this is followed by plastic hinges of the foot of the ground story columns. In this figure, the red line shows that the plastic hinges are not formed properly.

In the graph presented in Figure 14, which is related to the energy design method, the area below the force-displacement curve is quite larger than in the previous case, and in the nonlinear mode, the nonlinear capacity of the members is being used more appropriately. Also, after the formation of plastic hinges of the two ends of the frame beams and the ground story column bases, the columns of the other stories have entered their own nonlinear area.

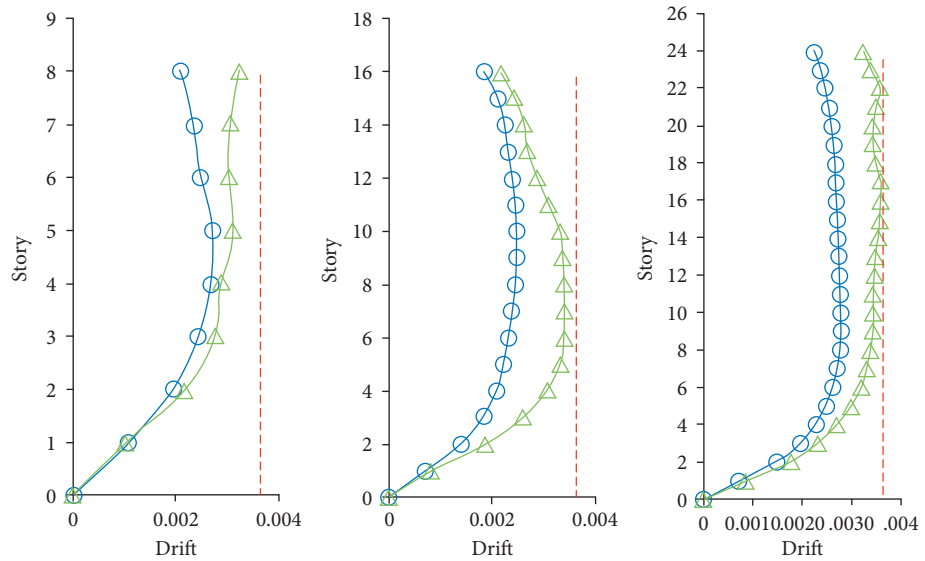

Figure 11: Comparing diagrams of the relative lateral displacement of 8-, 16-, and 24-story buildings.

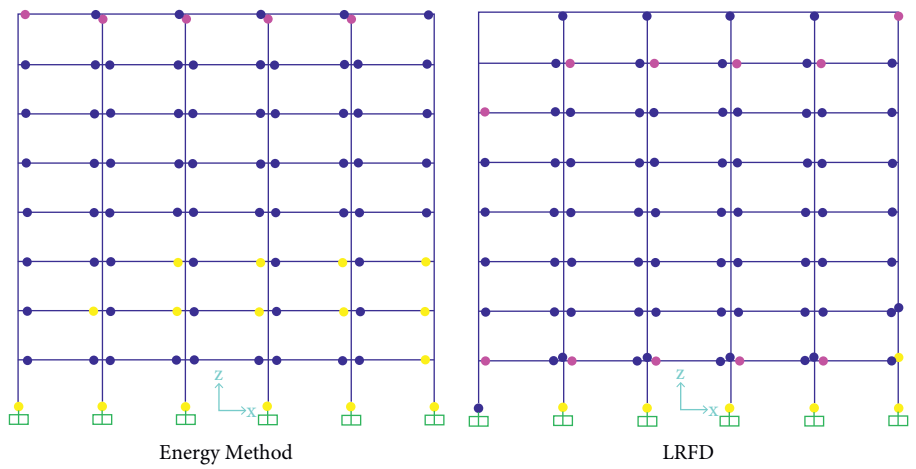

Figure 12: Plastic hinge created on an 8-story frame designed by the energy and LRFD methods.

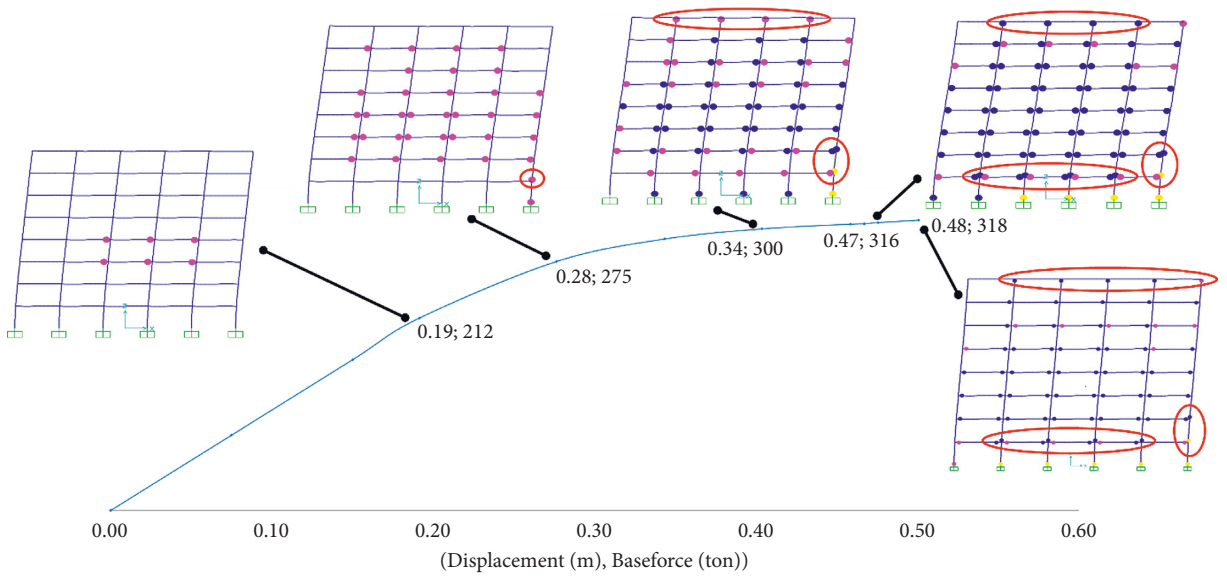

Figure 13: Pushover graph of an 8-story frame designed by the LRFD method.

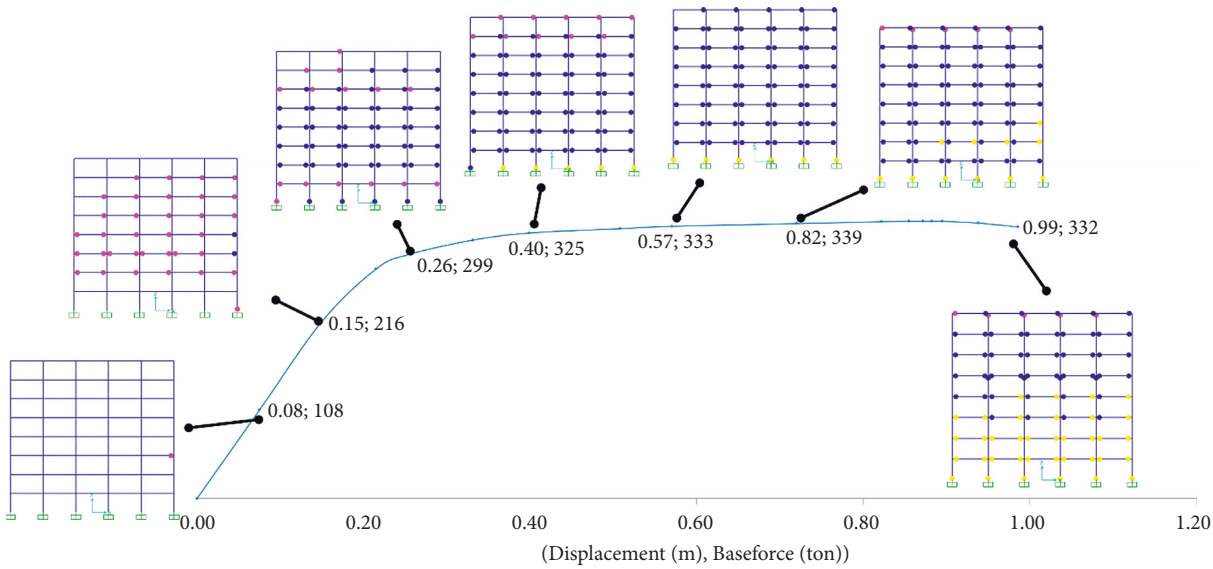

Figure 14: Pushover graph of an 8-story frame designed by the energy method.

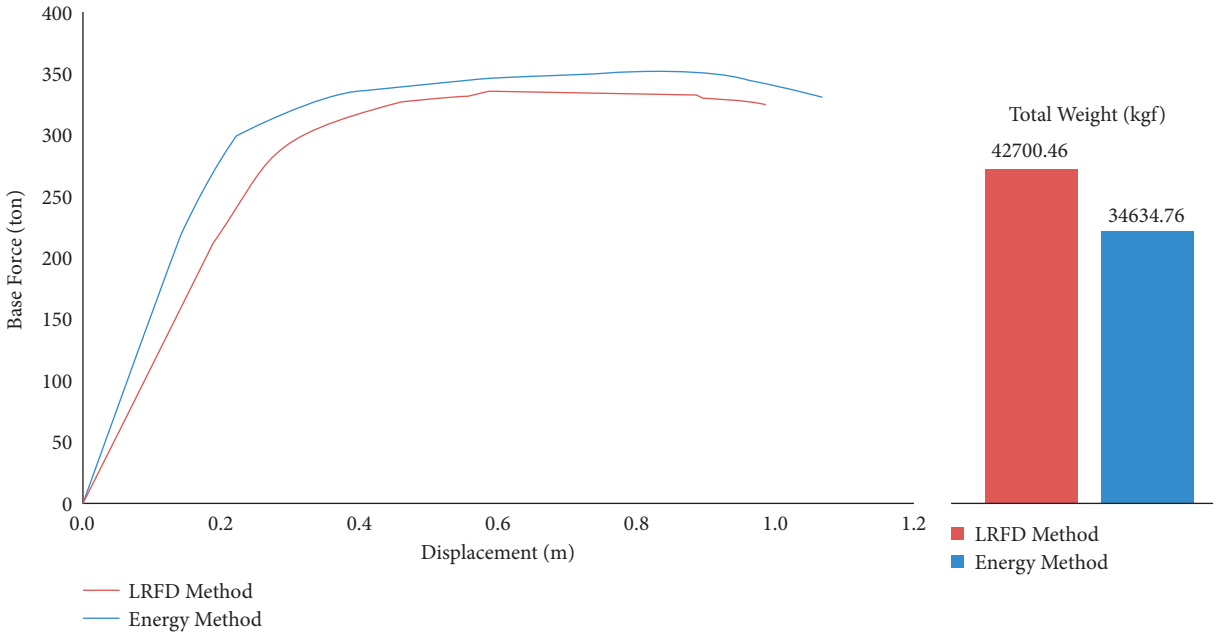

Figure 15: Comparing the push diagrams and the weight of the 8-story steel frame designed by the energy and LRFD methods.

As can be seen in Figures 13 and 14, in the target displacement of the 8-story frame, which is 0.35 m, for the frame which is designed by the energy method, the formation of plastic hinges is expanded in higher stories and beams. However, in the frame designed by the LRFD method, with the plastic hinge formation in the upper stories' columns, a local mechanism has been created, reducing the resistance. In Figure 15, which represents the push diagram of LRFD methods, energy along with the structure's weight is compared. The structure's weight by energy method is 34.634 tons, which is lower than that of the LRFD method with a weight of 42.7 tons. In the frame designed by the energy method, the surface below the frame diagram is larger than that of the LRFD method, thus showing that the energy method has used the nonlinear capacity of the members more appropriately.

5.2. Second Example: 16-Story Frame. Figure 16 shows the plastic hinges created in the 16-story frames, designed by the energy and LRFD methods.

Figures 17 and 18 have been used to better understand how plastic hinges are formed in the frames. In these figures, on the push diagram, the images related to plastic hinge formation in different stages are shown.

Figure 17 represents the diagram of a frame designed by the LRFD method. In this diagram, the poor performance of

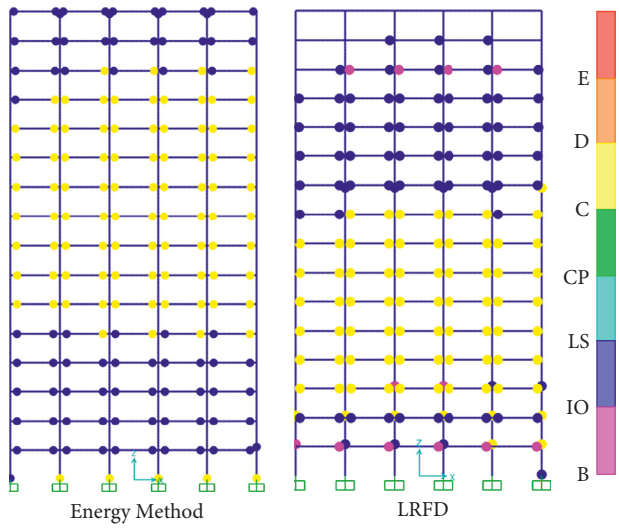

Figure 16: Plastic hinges created in the 16-story frames designed by the energy and LRFD methods.

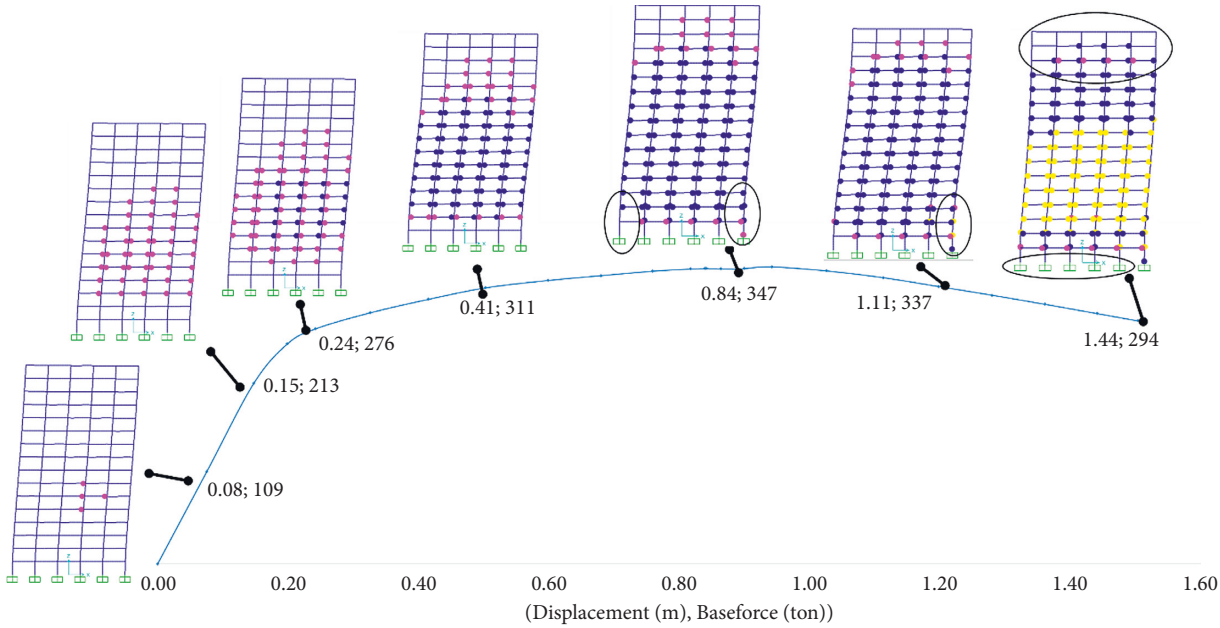

Figure 17: Push diagram of the 16-story frame designed by the LRFD method.

the frame in the nonlinear range can be seen. Also, beyond the 40 cm deformation of the roof, plastic hinges have been formed in many columns of the second story. Then, the plastic hinges have been created in the middle stories. In this diagram, it can be seen that some of the beams in the upper story and the base of the ground story columns still maintain their linear state, thus indicating the weakness of the LRFD method in the optimal use of the member's capacity.

Figure 18 shows the push diagram along with the steps of plastic hinges of the members in the frame designed by the energy method. In this figure, as can be seen, the area below the force-displacement diagram of the frame is quite large, and in the nonlinear mode, the energy design method uses the nonlinear capacity of the members more appropriately. Also, the columns did not enter their nonlinear state until the plastic hinges were formed in the beams at the two ends of the frame and the ground story columns.

As can be seen in Figures 17 and 18, in the target displacement of the 16-story frame, which is 0.6 m, like the 8-story one, for the frame designed by the energy method, plastic hinge formation is expanded in the upper stories and in the beams. However, in the frame designed by the LRFD method, due to the plastic hinge formation in the columns of the upper stories, a local mechanism has been created, thus reducing the strength. Meanwhile, in the structure, which is designed by the energy method, the plastic hinge formation at the columns' foot indicates that the capacity of the structure is used more extensively.

Figure 19 shows a comparison of the energy and weight of the 16-story structure designed by two methods. The

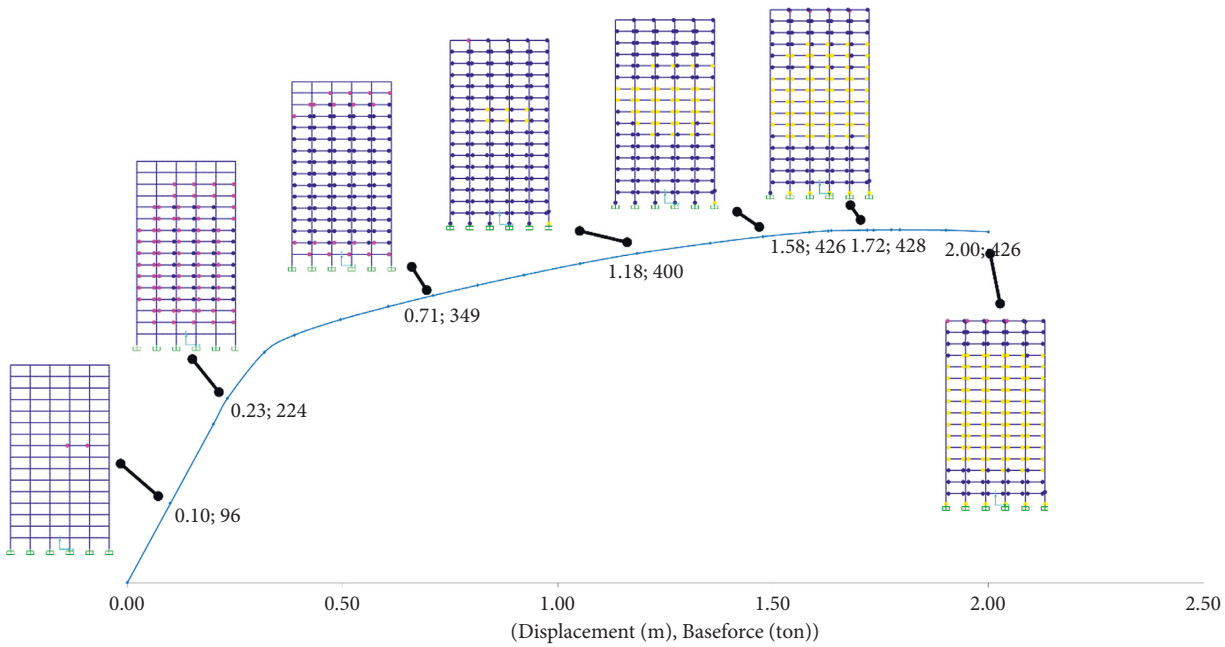

Figure 18: Push diagram of the 16-story frame designed by the energy method.

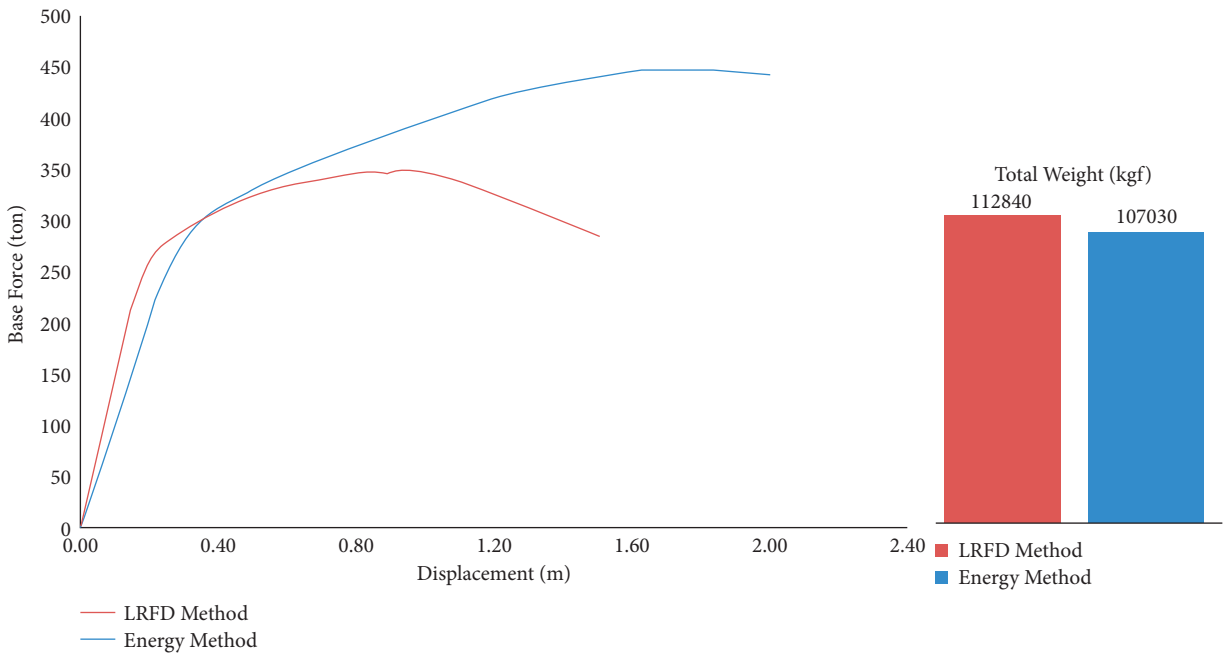

Figure 19: Comparing the push diagram and weight of the 16-story steel frame designed by the energy and LRFD methods.

structure's weight by the energy method is 107.030 tons, which is slightly lower than that of the LRFD method (112.840 tons). Also, in the frame designed by the energy method, the area below the force-displacement diagram is larger than that of the LRFD method, thus showing that the energy method has used the nonlinear capacity of the members more appropriately.

5.3. Third Example: 24-Story Frame. Figure 20 shows the plastic hinges created in the 24-story frames designed by the energy and LRFD methods.

Figures 21 and 22 help to better understand how plastic hinges are formed in the frames. In these figures, on the push diagram, the images of plastic hinge formation in different stages are shown.

Figure 21 represents the diagram of a frame designed by the LRFD method. In this diagram, the poor performance of the frame in the nonlinear range can be seen. It is worth noting that, beyond the target displacement of the roof, plastic hinges are formed in almost all columns of the second story. Then plastic hinges are created in the columns of the middle stories. In this diagram, it can be seen that some of

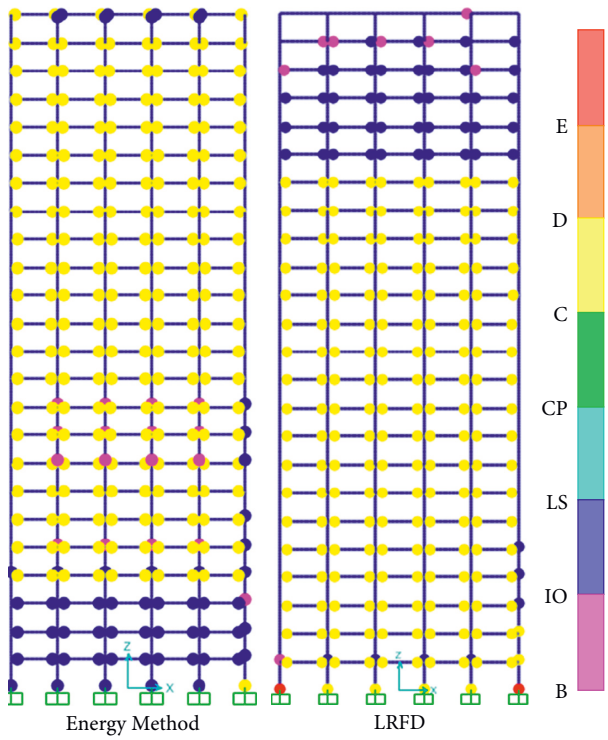

Figure 20: Plastic hinges created in the 24-story frames designed by the energy and LRFD methods.

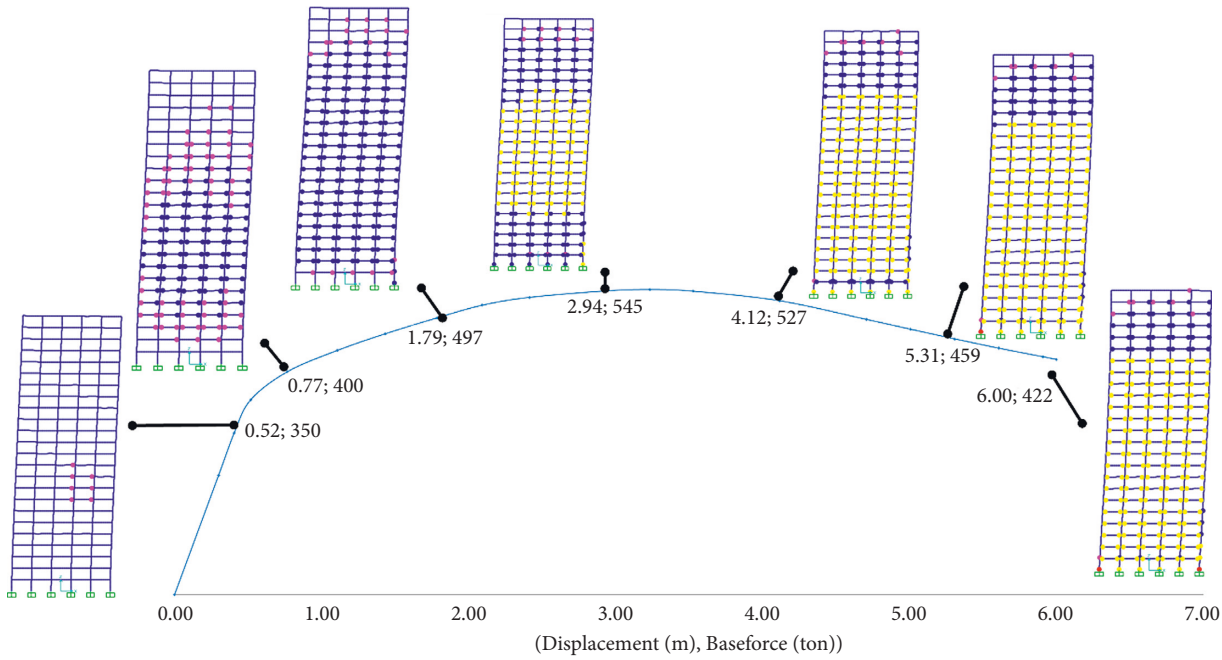

Figure 21: Push diagram of a 24-story frame designed by the LRFD method.

the beams in the upper story and the footings of the ground story columns still maintain their linear state, thus indicating the weakness of the LRFD method in the optimal use of the member's capacity.

Figure 22 shows the push diagram along with the steps of plastic hinges formed in the members of the frame designed by the energy method. In this figure, as can be seen, the area below the push diagram of the frame is larger, and in the nonlinear mode, the energy design method uses the nonlinear capacity of the members more extensively. It is notable that the columns did not enter their nonlinear area until the plastic hinges were created in the beams at the two ends of the frame and at the base of the ground story columns.

As can be seen in Figures 20 and 21, in the target displacement of the 24-story frame, which is 0.9 m, such as the

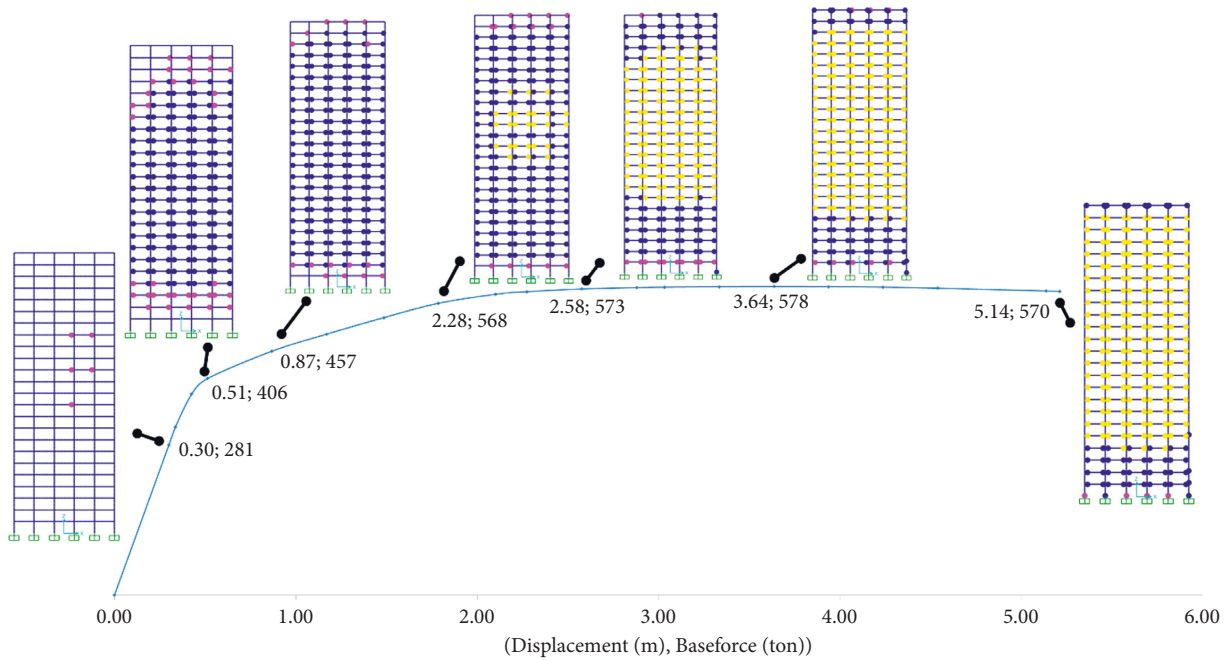

Figure 22: Push diagram of the 24-story frame designed by the energy method.

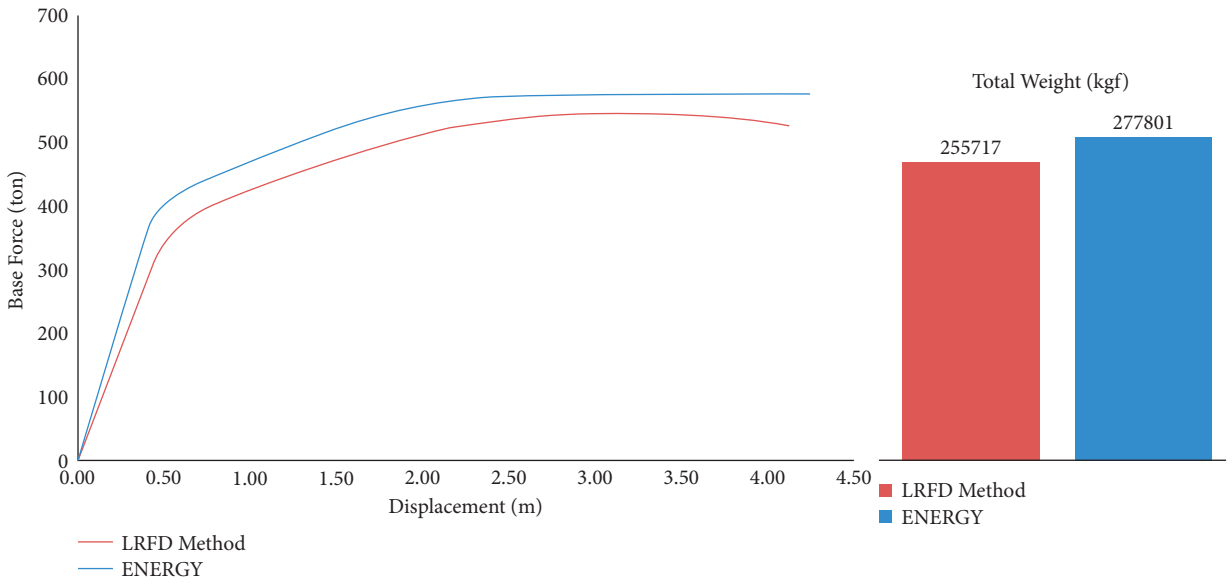

Figure 23: Comparing the push diagram and weight of the 24-story steel frames designed by the energy and LRFD methods.

8- and 16-story buildings, for the frame designed by the energy method, the plastic hinge formation was expanded in the upper stories and beams. However, in the frame designed by the LRFD method, due to the plastic hinge formation in the columns of the upper stories, a local mechanism has been created, reducing the strength. It is worth noting that, in the structure designed by the energy method, the plastic hinge formation at the columns foot indicates that the capacity of the structure is used more extensively.

Figure 23 compares the push diagrams of the structure designed by LRFD and the energy methods. Although the weight of the structure by the energy method (277.801 tons) is slightly higher than that of the LRFD method (255.717 tons), the nonlinear state and the energy absorption level of the former are better, showing that the LRFD method has not well used the capacity of its structural members.

6. Conclusion

In this paper, based on the modified equilibrium energy method, a new formulation is proposed for design of moment frames subjected to seismic loading. The damping effect of hysteresis cycles, the effects of different modes on the seismic input energy, the $P-\Delta$ effects, and the target

displacement have been seen in the formulation. Furthermore, the correction factor, as the ratio of the energy absorbed by the inelastic system to that of the equivalent elastic system, has been considered.

In this paper, 8-, 16-, and 24-story frames with lateral force resisting system of special steel moment frames have been designed by the proposed modified energy methods, as well as the design force method, according to AISC2016 code. Performance level criteria of ASCE41-17 code have been applied in a nonlinear analysis and design based on the desired performance of the frames. The results showed the following:

(i) The distribution of the plastic hinges in the frames designed by the proposed energy method was more desirable than that in the frames designed by the LRFD method.

(ii) For the frame, which is designed by the proposed energy method, the plastic hinges are formed and expanded in the upper stories and beams. However, for the frame, which is designed by the LRFD method, the plastic hinges are created in the columns of the upper stories, and a local mechanism is formed.

(iii) For the structure designed by the energy method, the formation of plastic hinges at the columns' foot indicates that the structure's capacity is used more.

(iv) A more uniform distribution of drift is seen in the structure, which is designed by the energy method compared to the LRFD method.

(v) In the 8- and 16-story structures, the weight of the structure, which is designed by the energy method, is less than that obtained by the LRFD method.

(vi) In the 24-story structure, a lower weight was obtained in the LRFD method as compared to the modified energy method.

(vii) The study showed that the relationships presented in the codes in regard to the Strong-Column Weak-Beam rule cannot prevent local and undesirable mechanisms in severe earthquakes. Meanwhile, in structures designed by the energy method, undesirable mechanisms did not occur.

In general, using the modifications made on the input-output energy balance relations applied to the structure, the modified energy method can lead to more favorable results in the optimal distribution of plastic hinges and seismic energy dissipation as compared to the LRFD method.

Data Availability

The data used to support the findings of the study can be obtained from the corresponding author upon request.

Conflicts of Interest

The authors declare that there are no conflicts of interest regarding the publication of this paper.

References

[1] G. W. Housner, "Limit design of structures to resist earthquakes," in *Proceedings of the 1st World Conference on Earthquake Engineering*, pp. 5.1–5.13, Oxford, England, March, 1956.

[2] H. Akiyama, *Earthquake-Resistant Limit-State Design for Buildings*, University of Tokyo Press, Tokyo, Japan, 1985.

[3] Fakhri-Niasar and Mohsen, "The energy spectrum of the Iranian earthquakes," Master of Science Thesis, Islamic Azad University, Science and Research Branch, Tehran, 1998.

[4] H. Maleki and M. Ghafory-Ashtiany, "Study on the energy of earthquakes in reinforced concrete moment frames," *Journal of Seismology and Earthquake Engineering*, vol. 3, no. No. 2, p. 11, 2000.

[5] A. Ruzi, "Energy concept in earthquake-resistant design," Master of Science Thesis, Istanbul Technical University, Department of Civil Engineering, 2003.

[6] F. Mollaioli and L. Decanini, "An energy-based methodology for the assessment of seismic demand," *Soil Dynamics and Earthquake Engineering*, vol. 21, no. 2, p. 25, 2001.

[7] L. Ye, G. Cheng, and Z. Qu, "Study on energy-based seismic design method and the application for steel braced frame structures," in *Proceedings of the Sixth International Conference on Urban Earthquake Engineering*, p. 12, Tokyo Institute of Technology, Tokyo, Japan, August, 2009.

[8] G. Ghodrati-Amiri, G. Abdollahzadeh-Darzi, and M. Khanzadi, "Earthquake duration and damping effects on input energy," *International Journal of Civil Engineering*, vol. 5, no. 1, p. 16, 2007.

[9] F. Haddad-Shargh and M. Hosseini, "An optimal distribution of stiffness over the height of shear buildings to minimize the seismic input energy," *Journal of Seismology and Earthquake Engineering (JSEE)*, vol. 13, no. 1, p. 8, 2011.

[10] G. Havaei and E. Mobedi, "Effect of interaction and rocking motion on the earthquake response of buildings," *Journal of Structural and Construction Engineering (JSCE)*, vol. 1, no. 1, p. 11, 2015 (In Persian).

[11] R. Bemanian and H. Shakib, "Evaluation of nonlinear behavior of dual steel frame-shear wall system by a group of real earthquakes," *Journal of Structural and Construction Engineering (JSCE)*, vol. 2, no. 4, p. 13, 2016.

[12] R. Vahdani, M. Gerami, and M. A. Vaseghi Nia, "Structural damping and displacement ductility effects on input energy spectrum of earthquake," *Journal of Structural and Construction Engineering*, vol. 5, no. 2, pp. 5–21, 2018.

[13] T. Ucar, "Computing input energy response of MDOF systems to actual ground motions based on modal contributions," *Earthq. Struct*, vol. 18, no. 2, pp. 263–273, 2020.

[14] T. T. Tran and B. Adhikari, "Energy based seismic design coefficients," in *AIP Conference Proceedings*, vol. 2420, AIP Publishing LLC, Article ID 020036, 2021.

[15] R. Bagherzadeh, A. Riahi Nouri, M. S. Massoudi, M. Ghazi, and F. Haddad Shargh, "AN effective hybrid method for optimizing steel frames with improved seismic performance," *Iran University of Science & Technology*, vol. 12, no. 3, pp. 365–398, 2022.

[16] A. Committee, *Seismic Provision for Structural Steel Buildings (ANSI/AISC 341-16)*, American Institute of Steel Construction, Chicago, 2016.

[17] ASCE, "ASCE/SEI 7-16 Minimum Design Loads for Buildings and Other Structures," *American Society of Civil Engineers*, vol. 2, 2016.

[18] I. MathWorks, *MATLAB and Statistics Toolbox Release 2012b*, I. MathWorks, Natick (Massachusetts, United States), 2012.
[19] CSI (Computers & Structures, Inc), *CSI Analysis Reference Manual for SAP2000 Ver*, CSI, Walnut Creek, CA, 2017.
[20] S. S. Lee, *Performance-based Design of Steel Moment Frames Using Target Drift and Yield Mechanism*, University of Michigan, Ann Arbor, Michigan, 2002.
[21] S. Leelataviwat, W. Saewon, and S. C. Goel, "Application of energy balance concept in seismic evaluation of structures," *Journal of Structural Engineering*, vol. 135, no. 2, pp. 113–121, 2009.
[22] C. M. Uang and V. V. Bertero, *Use of energy as a design criterion in earthquake-resistant design*, vol. 88, Earthquake Engineering Research Center, University of California, Berkeley, California, 1988.
[23] N. M. Newmark and W. J. Hall, *Earthquake Spectra and Design. Engineering Monographs on Earthquake Criteria*, Earthquake Engineering Research Institute, Oakland, CA, 1982.
[24] J. Bai and J. Ou, "Plastic limit-state design of frame structures based on the strong-column weak-beam failure mechanism," in *Proceedings of the 15th World Conference on Earthquake Engineering*, Lisbon, Portugal, September, 2012.
[25] G. Manfredi, "Evaluation of seismic energy demand," *Earthquake Engineering & Structural Dynamics*, vol. 30, no. 4, pp. 485–499, 2001.
[26] S. Leelataviwat, S. C. Goel, and B. Stojadinović, "Toward performance-based seismic design of structures," *Earthquake Spectra*, vol. 15, no. 3, pp. 435–461, 1999.
[27] H. M. Dwairi, M. J. Kowalsky, and J. M. Nau, "Equivalent damping in support of direct displacement-based design," *Journal of Earthquake Engineering*, vol. 11, no. 4, pp. 512–530, 2007.
[28] S.-S. Lee, S. C. Goel, and S.-H. Chao, "Performance-based Design of Steel Moment Frames Using Target Drift and Yield Mechanism," Report No. UMCEE 01-17, Department of Civil and Environmental Engineering, University of Michigan, Ann Arbor, Michigan, 2001.
[29] Asce 41-17, *Seismic Evaluation and Retrofit of Existing Buildings*, American Society of Civil Engineers, Reston, Virginia, 2017.